Ultramicroscopy 253 (2023) 113819

Contents lists available at ScienceDirect

Ultramicroscopy

journal homepage: www.elsevier.com/locate/ultramic

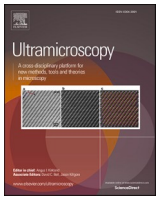

Methodology and implementation of a tunable deep-ultraviolet laser source for photoemission electron microscopy

Andrew J. Winchester [a], Travis J. Anderson [b], Jennifer K. Hite [b], Randolph E. Elmquist [c], Sujitra Pookpanratana [a,*]

[a] Nanoscale Device and Characterization Division, National Institute of Standards and Technology, Gaithersburg, MD, United States
[b] Electronics Science and Technology Division, U.S. Naval Research Laboratory, Washington, DC, United States
[c] Quantum Measurement Division, National Institute of Standards and Technology, Gaithersburg, MD, United States

ARTICLE INFO

Keywords:
Photoemission electron microscopy
Space charge
Deep ultraviolet
Ultrafast laser

ABSTRACT

Photoemission electron microscopy (PEEM) is a unique and powerful tool for studying the electronic properties of materials and surfaces. However, it requires intense and well-controlled light sources with photon energies ranging from the UV to soft X-rays for achieving high spatial resolution and image contrast. Traditionally, many PEEMs were installed at synchrotron light sources to access intense and tunable soft X-rays. More recently, the maturation of solid-state lasers has opened a new avenue for laboratory-based PEEMs using laser-based UV light at lower photon energies. Here, we report on the characteristics of a laser-based UV light source that was recently integrated with a PEEM instrument. The system consists of a high repetition rate, tunable wavelength laser coupled to a harmonics generation module, which generates deep-UV radiation from 192 nm to 210 nm. We comment on the spectral characteristics and overall laser system stability, as well as on the effects of space charge within the PEEM microscope at high UV laser fluxes. Further, we show an example of imaging on gallium nitride, where the higher UV photon energy and flux of the laser provides considerably improved image quality, compared to a conventional light source. These results demonstrate the capabilities of laser-based UV light sources for advancing laboratory-based PEEMs.

1. Introduction

The illumination source is important for microscopy and is always a major factor in determining what can be seen. This is critical for photoemission-based methodologies, such as photoemission electron microscopy (PEEM), where energetic light is required to eject a photoelectron for detection. PEEM is a multi-modal microscopy technique that operates by using a system of electromagnetic lenses to collect and image photoelectrons emitted via the photoelectric effect from a sample surface [1,2]. The emitted electron has a kinetic energy (E_{kin}) and maximum momentum (k) given by

$$E_{kin} = h\nu - \varphi - E_B \tag{1}$$

$$k = \frac{\sqrt{2mE_{kin}}}{\hbar} \tag{2}$$

Here, $h\nu$ is the photon energy of the incident light, φ is the work function, E_B is the bound energy of the electron before it left the material, m is the free electron mass, and $\hbar$ is the reduced Planck constant. Hence, photons with energy greater than the sample work function, typically from 3 eV to 6 eV, are needed to begin ejecting photoelectrons from the Fermi level ($E_B = 0$). Further, the photon energy will dictate the studies that can be performed using PEEM. Photon energies in the deep ultraviolet (DUV, typically 4 eV to 6 eV) give photoemission contrast related to dissimilar work function, ionization potential (IP), or density of states (DOS) near the Fermi energy. Higher photon energies (10 eV to 100 eV) allow for probing the complete electronic band structure of surfaces where the photoionization cross section is at a maximum[3], while soft X-rays (100 eV to 1000 eV) are able to photoemit elemental

Abbreviations: Photoemission electron microscopy, (PEEM); Deep ultraviolet, (DUV); Ionization potential, (IP); Density of states, (DOS); Second harmonic, (2ω); Third harmonic, (3ω); Fourth harmonic, (4ω); Fundamental, (ω); Fused silica, (FS); Neutral density, (ND); De-ionized, (DI); Field of view, (FOV); Full width at half maximum, (FWHM).

* Corresponding author.
E-mail address: sujitra@nist.gov (S. Pookpanratana).

https://doi.org/10.1016/j.ultramic.2023.113819
Received 9 December 2022; Received in revised form 21 June 2023; Accepted 25 July 2023
Available online 26 July 2023
0304-3991/Published by Elsevier B.V.

core electrons, providing chemically-insightful PEEM images of differentiating materials and composition [1,2].

In addition to the photon energy, other essential characteristics of the light source for PEEM are monochromaticity, high photon flux, and continuous wave or high repetition rate (> 1 MHz) operation. Lab-based light sources for PEEM have traditionally been based on gas (He, Hg, Xe) discharge lamps, where the available photon energy is limited to discrete electronic transitions. Third and fourth generation synchrotrons with high intensity and tunable light (vacuum-UV to soft X-rays) are a critical base for performing photoemission and have enabled many advanced PEEM measurements [1,2]. Still, there is a strong desire to develop and implement novel photon sources for lab-based measurements to complement synchrotron sources, such as for performing non-linear photoemission and studying ultrafast dynamics.

In recent years, the development and maturation of solid state ultrafast pulsed lasers has resulted in increased use of laser-based photon sources for photoemission [4]. Key developments that have enabled the use of ultrafast pulsed lasers are high average powers and high repetition rates, where the former is important for maximizing photon flux from non-linear photon generation schemes and the latter is crucial for achieving sufficient measurement statistics. Generating DUV and vacuum-UV photons from pulsed sources is commonly achieved through non-linear frequency conversion schemes, such as frequency doubling and quadrupling of near-infrared lasers in birefringent crystals [5,6]. For example, 266 nm (4.65 eV, 3rd harmonic) and 200 nm (6.2 eV, 4th harmonic) light can be readily produced through frequency doubling and mixing of 800 nm (1.55 eV) light from Ti:Sapphire lasers. Mature Ti:Sapphire technology offers several attractive properties for PEEM: high repetition rate (≈ 80 MHz) oscillator lasers, tunable output (700 nm to 1000 nm), sufficient pulse energy for frequency conversion, and good laser stability and beam properties. Consequently, laser-driven light sources for laboratory-based PEEMs have seen increasing usage over the last decade [7,8,17,18,9–16].

Early integration of high pulse energy ultrafast lasers in PEEM experiments suffered from severe space charge effects, which resulted in signal degradation due to the low repetition rates of the laser systems [19–22]. Space charge is the result of multiple photoelectrons interacting with each other via Coulomb repulsion as they propagate from the sample surface to the detector. Tightly grouped electron bunches emitted by short and intense light pulses can result in significant distortion and degradation of the spatial, momentum, and energetic information carried by the electrons [23].

Space charge effects were studied previously in several different PEEM and light source configurations. In a PEEM with a hemispherical energy analyzer using a femtosecond pulsed amplified laser at moderate repetition rates (100 kHz and 250 kHz), space charge effects were observed and the authors argued that a significant portion of the space charge effect could arise at the entrance to the energy analyzer, where the propagating electrons are slowed down to 1250 eV from the initial 20 keV acceleration voltage [19]. At synchrotron light sources, space charge effects were studied under high photon flux and high repetition rate (500 MHz) conditions in the soft X-ray regime, where many electrons over a wide energy range can easily be liberated by a single light pulse [24,25]. Space charge effects were also observed in a PEEM using an in-line omega filter, where no deceleration in the energy analyzer is present [25], suggesting that the majority of the space charge interaction happens during the initial acceleration of electrons from the sample surface. More recently, a novel gas discharge vacuum UV light source was investigated, which produces relatively long pulses (10s of ns) at a low repetition rate (few kHz) [26]. The space charge effects were severe despite the long pulses, indicating that the photoelectrons underwent significant Coulomb interaction as they left the sample surface and at trajectory cross over points within the PEEM. Ultimately, space charge in PEEM must be minimized to maximize the reliability and accuracy of measuring the position, energy, and momentum of the photoelectron, which in practice means reducing the number of photoelectrons generated per excitation pulse [19,24–26]. This implies that the number of pulses per unit time (repetition rate) should be as high as possible to maintain signal quality. The previous studies on space charge in PEEM have examined lower repetition rate regimes with short [19] and long [26] pulses and higher repetition rates with moderate pulse durations at synchrotron sources [24,25]. However, there has been no report on the extent of space charge effects in PEEM using high repetition rate femtosecond pulsed lasers.

Here, we report on the successful integration of a high repetition rate, ultrafast DUV source to a PEEM instrument. The laser system consists of a wavelength-tunable, 80 MHz Ti:Sapphire laser driving a harmonic generation module to produce tunable DUV output wavelengths as short as 192 nm. The optical output from this laser system is then coupled to a PEEM, and to the best of our knowledge, this unique set-up is the first of its kind. We show that the laser system provides good performance, in terms of tunability, spectral quality, photon flux, and stability. We then show initial PEEM results on the effects of space charge in the system at high repetition rates, as well as the improved imaging quality over a conventional light source for wide bandgap semiconductors. The combination of high photon flux and continuous tunability with mostly automated wavelength control represents an evolutionary step in access and reliability to high-intensity light sources for laboratory-based PEEMs.

2. Materials and methods

2.1. Laboratory conditions for instrumentation

The PEEM and laser optics (i.e., optical table) are both located at ground level in the Advanced Measurement Laboratory building in Gaithersburg, MD. The horizontal and vertical floor vibrations are less than 1 μm s^{-1} and 3 μm s^{-1}, respectively, for frequencies between 1 Hz and 1000 Hz. The PEEM table is passively dampened. The PEEM and optical table are not connected and are used without air floating to maintain repeatable coupling of the laser into the PEEM without active laser beam stabilization. The laboratory is temperature and humidity controlled to within 0.25 °C and 5% relative humidity, respectively.

2.2. Laser setup to the PEEM

The layout of the optical setup is illustrated in Fig. 1a. The laser source is a tunable Ti:Sapphire oscillator laser (Chameleon Ultra II, Coherent [27]), which outputs approximately 3.5 W average power with a 140 fs pulse duration at an 80 MHz repetition rate. The center wavelength can be tuned via computer control between 680 nm and 1080 nm. The laser output is directed via two mirrors through a broadband Faraday isolator and half-waveplate before entering the harmonic generation module. The Faraday isolator prevents back-reflections from the harmonics module from entering the laser, which was found to be crucial for achieving stable operation of the system across the wavelength tuning range.

The harmonics module (HarmoniXX, APE [27]) generates the second (2ω), third (3ω), and fourth (4ω) harmonics of the fundamental (ω) from the Ti:Sapphire laser. The module uses a non-linear frequency doubling and mixing scheme to generate the 4ω via mixing 3ω with the laser fundamental (i.e., $4\omega = 3\omega + \omega$), similar to other reported optical setups [5,6]. Most of the critical optics in the module are motorized and can be computer controlled.

The 4ω output of the module is directed towards a periscope, as shown in Fig. 1b, which raises the beam height by 25 cm to match that of the sample stage in the PEEM. The beam passes through a diaphragm iris before reaching a fused silica (FS) lens (500 mm focal length), which focuses the 4ω beam though a MgF_2 conflat window into the PEEM and onto the sample at normal incidence, as shown in Fig. 1c. The laser power sent into the PEEM can be attenuated by a variable neutral density (ND) filter wheel before the periscope that reflects a portion of

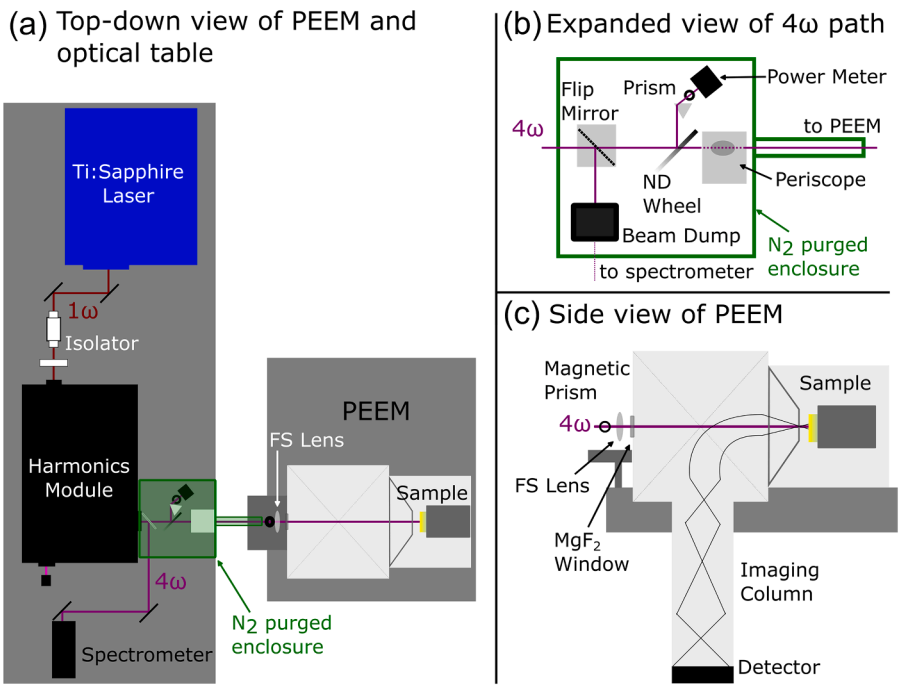

Fig. 1. Optical layout of DUV laser system and PEEM. Top-down view a) of laser and PEEM tables and b) zoomed-in view of N_2 purged box and tube in (a), showing the 4ω beam path as it passes a motorized flip mirror and neutral density (ND) wheel before entering a periscope to match the PEEM height. The path length from the laser output to the harmonics module output is approximately 205 cm and the path length from the harmonics module to the sample in the PEEM chamber is approximately 168 cm, giving a total optical path length of 373 cm for the experiment. c) Side-view of PEEM, showing the 4ω beam (in purple) through the iris, fused silica (FS) lens and MgF_2 window prior to entering the vacuum chamber and the path of photo-emitted electrons in the microscope imaging column (black lines) emitted from the sample (yellow rectangle) illuminated by 4ω light.

the beam, as shown in Fig. 1b. The reflected portion is dispersed through a prism to spatially separate residual ω and 3ω backgrounds from the 4ω, which is directed through a diaphragm iris onto an optical power meter. This allows for accurately monitoring the 4ω intensity and is an essential aid when optimizing the 4ω after changing the laser wavelength. The beam can be intercepted before the periscope by a motorized flip mirror to direct the beam either to a spectrometer for diagnostics, or to a beam dump. The optical setup between the 4ω output from the harmonics module and the window of the PEEM is enclosed within an acrylic box and tube which are purged with N_2 to reduce absorption of the UV light by oxygen and water and prevent ozone generation. The box also provides protection against any stray UV light to laboratory occupants and minimizes the effects of air currents on the beam stability.

2.3. PEEM experimental conditions

The PEEM is a commercial system without aberration correction (SPECS GmbH [27–29]) and the PEEM set-up before laser installation has been previously described [30]. The system has a magnetic prism array for energy selection (Fig. 1c) and does not have an electron gun. The base pressure of the analysis chamber was better than 10^{-9} mbar. The acceleration voltage was 15 kV for all PEEM experiments, and the turbomolecular pumps in the vacuum system remained on while acquiring all PEEM images. PEEM images were either acquired using the DUV laser source or a conventional mercury arc source. All images were corrected for detector non-uniformity using a standard flat-field and dark image method. All PEEM images were corrected for position or energy drift before averaging the individual frames.

An epitaxial graphene on SiC sample [31] was used for the measurements in Section 3.2.1. The sample was outgassed briefly in-situ at approximately 500 K before experiments. A spatial aperture was used in the diagonal plane of the PEEM magnetic prism to select a 7.4 μm area of the sample for spectroscopy. A 2 μm wide slit was inserted at the PEEM magnetic prism entrance to give an energy resolution of approximately 350 meV, and the dispersed energy spectrum was projected onto the detector. The 4ω wavelength was 200 nm (6.2 eV). The image exposure time was 10 s with 20 frames averaged at a detector voltage of 1400 V.

The sample for the PEEM images in Section 3.2.2 was p-type GaN grown on an unintentionally doped GaN buffer on an n-type GaN substrate[32]. The sample was ex-situ cleaned in the following sequence: ultrasonicated in acetone (5 min), ultrasonicated in isopropanol (5 min), placed in piranha solution (3:1 by volume H_2SO_4:H_2O_2, 15 min), rinsed with deionized (DI) water, placed in HCl (9.45 mol L^{-1}, 15 min) and rinsed with DI water. The sample was immediately loaded into the PEEM and outgassed at 500 K for 30 min, then briefly annealed at 800 K for a few minutes.

The low magnification image in Fig. 4a was taken with the mercury arc source at a 100 μm field of view (FOV) and camera exposure times of 10 s with 100 frames averaged at a detector voltage of 1400 V. The images in Fig. 4b and Fig. 4c were taken with 4ω (200 nm, 0.37 nJ cm^{-2} fluence). The 50 μm FOV image in Fig. 4b was acquired with a camera exposure time of 2 s with 50 frames averaged and detector voltage 1300 V. The high magnification image in Fig. 4c was taken with a 3 μm FOV, exposure time of 5 s with 100 averages, and a detector voltage of 1400 V. Large selected area (14.8 μm projected) and contrast (100 μm) apertures were used to eliminate lens crossover artifacts at high magnification. Images were corrected for exposure time and detector gain differences.

3. Results and discussion

3.1. Setup characteristics

We first discuss the characteristic parameters and performance of the laser and 4ω generation. As described in Section 2.2, the laser is tunable between 680 nm and 1080 nm. However, the achievable 4ω wavelength depends strongly on the phase matching conditions of the non-linear crystals used for frequency mixing, as well as the UV absorption of the crystals [5,6]. For the current harmonics module configuration, the phase matching conditions can be realized for fundamental wavelengths from approximately 760 nm to 840 nm, with resulting 4ω wavelengths between 190 nm (6.5 eV) and 210 nm (5.9 eV). Several ω and corresponding 4ω spectra are shown in Figs. 2a and 2b, respectively.

Typically, using the full fundamental input power (≈ 3.5 W), we obtain average 4ω powers of approximately 2 mW to 10 mW between 192 nm and 210 nm, giving an overall conversion efficiency on the order of 0.1%. While shorter wavelengths (e.g., 190 nm) can be achieved, it is more difficult to align and optimize the 4ω due to the lower conversion efficiency at this limit [5,6]. The obtained average 4ω powers

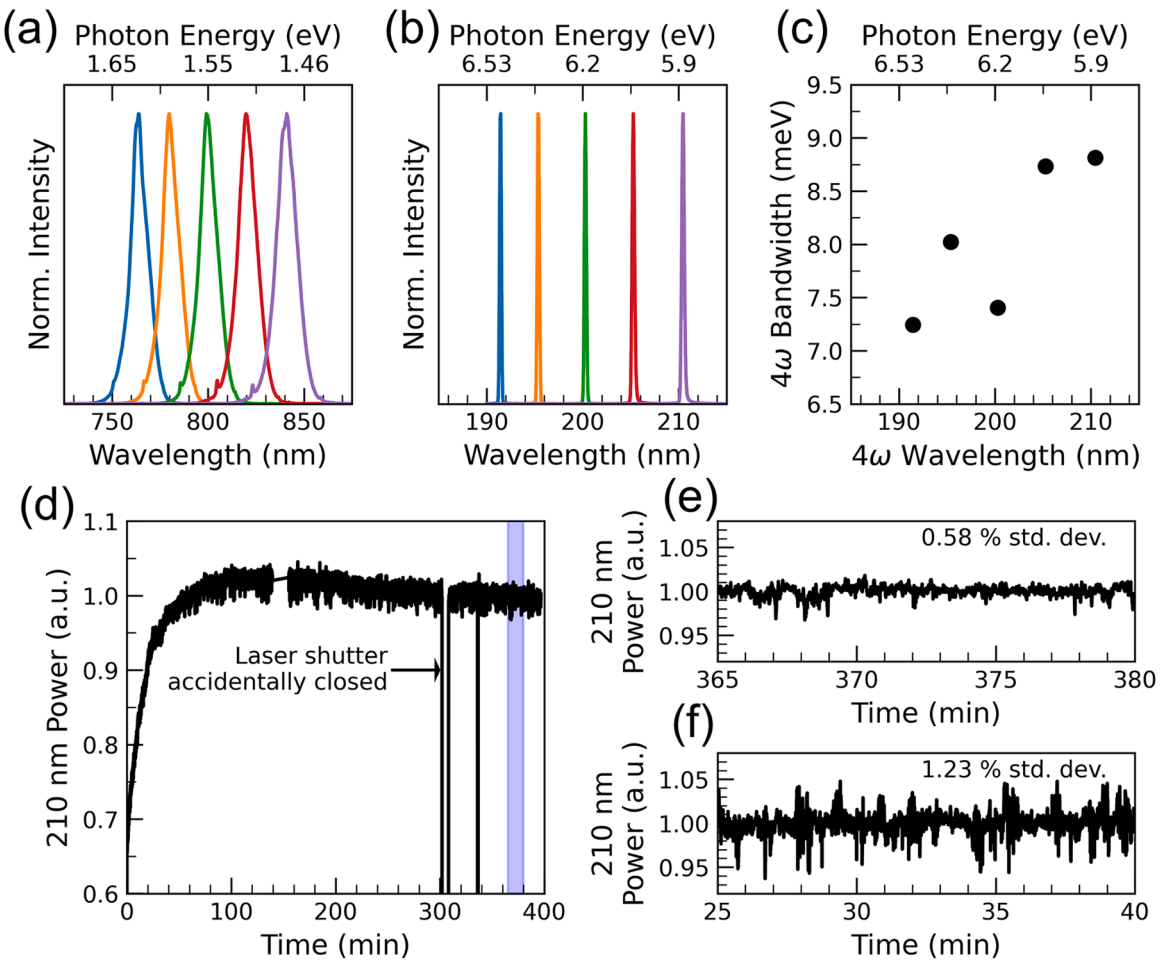

Fig. 2. Laser and 4ω characteristics. a) Fundamental laser spectrum at several wavelengths and b) corresponding 4ω spectra. c) Energy bandwidths (FWHM) of the 4ω spectra at different wavelengths. d) Normalized 4ω power at 210 nm as a function of time after turning on the laser system. The sharp dips at around 300 min and 340 min are due to accidental activation of the lab interlock system, causing the laser shutter to close during logging. e) Short-term power stability of the 4ω at 210 nm after the system has stabilized, taken from the blue shaded region in d). In f), power stability shortly after changing the operating wavelength.

correspond to a total pulse energy and photon flux on the order of 10^{-11} J and 10^{15} photons s^{-1}, respectively.

The energy bandwidths of the 4ω light, taken from the full width at half maximum (FWHM) of the spectra in Fig. 2b, are found to be in the range of 7 meV to 9 meV, as shown in Fig. 2c. This energy bandwidth is considerably smaller than the PEEM instrument energy resolution (≈ 200 meV). Interestingly, it is also narrower than the fundamental laser output (approximately 24 meV), which confirms that the non-linear crystals in the harmonics module have been chosen to optimize output power instead of maintaining a shorter pulse duration [6], where the former is an initial priority for PEEM measurements. From the measured 4ω spectrum, we can estimate the Fourier-transform limited pulse duration to be approximately 230 fs. However, the laser fundamental itself is not Fourier-transform limited, and the ratio of the pulse width determined from autocorrelation to that from the spectral width is roughly a factor of two. Therefore, we expect that the 4ω light is also not Fourier-transform limited, and likely closer to 500 fs, as there is no dispersion compensation in the optical setup.

In addition to the 4ω photon energy (or wavelength) and intensity characteristics, the stability of the source over time is also important to consider for photoemission measurements. Since multiple non-linear processes are cascaded to generate the 4ω light, small fluctuations in the laser output or laboratory ambient conditions could have significant contributions to the power stability and noise level. The laboratory containing the PEEM and DUV laser system is temperature controlled to less than 0.25 °C fluctuations, which minimizes environmental effects. The main contributions to the 4ω stability come directly from the laser, its associated thermal load on optical components, and the alignment of the harmonics box.

Evaluating the 4ω power at 210 nm after the system has stabilized for an hour (Fig. 2d), we measure a standard deviation of the fluctuation in power of 0.58% over 15 min, as shown in Fig. 2e. Given that the laser output standard deviation is around 0.1% or better, which corresponds to a theoretical standard deviation fluctuation of 0.4% for correlated noise, this 4ω power output fluctuation of 0.58% is very promising. However, we note that reaching this level of fluctuation takes some diligence with alignment and patience for the system to reach stability. For example, to change the wavelength of the system, it requires optimization of several optical components inside the harmonics module. As shown in Fig. 2f, the power output fluctuations are worse shortly after changing the operating wavelength. The measurement shown in Fig. 2d and Fig. 2f were taken with the same optical alignment (without any adjustments), but the data in Fig. 2d was taken three days after Fig. 2f. This indicates that the optical components require time to settle into a stable configuration after large wavelength changes. The fluctuation in this case is approximately 1.2% standard deviation, which is still acceptable for most PEEM measurements, but this may cause issues when the intensity stability is crucial. Overall, there is relative ease in changing the 4ω output wavelength, which is an important modality in PEEM for enhanced sensitivity to differences in the inelastic mean free path of photoelectrons and local electronic structure (e.g., work functions and valence band edges).

3.2. Laser-based PEEM results

Upon sending the 4ω beam into PEEM, we can achieve a spot size of approximately 240 μm diameter (e^{-2}) on the sample by partially restricting a diaphragm iris just before the FS lens. For this moderate spot size, we were not able to detect any beam motion on the sample in the PEEM, indicating that the beam pointing stability is better than a few tens of micrometers for our experimental layout. The spot profile is improved when closing the iris, indicating that the 4ω beam quality is not ideal, which is expected due to beam depletion during multiple stages of non-linear mixing. This is confirmed by an estimated M^2 value of 2 for an approximately 1 mm diameter beam at the lens with the iris closed. Even at this modest focusing condition, we find that the total available 4ω photon flux is orders of magnitude too high for PEEM measurements. The photoelectrons generated from the 4ω maximum output power is too much for the PEEM electron detector screen to safely handle at lower magnifications. However, the detector is not usually the limiting factor for the usable photon flux. Space charge effects from multiple electrons emitted by a single laser pulse limit the maximum useful photoelectron signal and will be discussed in the following Section 3.2.1.

3.2.1. Space charge and usable photon flux

Here, we characterize the influence of photon flux to understand the working conditions for our PEEM measurements using the high-repetition rate laser source. The effects of space charge in the PEEM were evaluated by measuring the photoemission spectrum at several laser fluences from an epitaxial graphene sample, where the measurement geometry is described in Section 2.3. As the laser fluence is increased, we first observe an increase in the peak photoemission intensity, where the increased photon flux corresponds to increased photoemission signal, as shown in Fig. 3a. Increasing the laser fluence further causes the photoemission intensity to begin saturating and eventually decrease as the spectrum broadens, as shown in the top-most spectrum in Fig. 3a. This broadening and redistribution of the photoelectron spectrum is due to the interaction of multiple electrons emitted in a single pulse; the electrons repel each other as they are accelerated from the sample surface and travel through the microscope, causing their kinetic energy, as well as momentum and spatial position, to change [19,24–26]. The FWHM of the spectra are shown in Fig. 3b to illustrate this point. For fluences less than approximately 2 nJ cm^{-2}, as indicated by the shaded blue area in Fig. 3b, the effect of space charge on the spectrum width is negligible within the energy resolution of the PEEM instrument.

This space charge limit corresponds to an average power and a photon flux of approximately 50 μW and 10^{13} photons s^{-1}, respectively, which is two orders of magnitude less than the typical 4ω output power of the harmonics module. This photon flux limit is consistent with reports from broadening with intense X-ray synchrotron illumination [24,25] as well as amplified femtosecond lasers [19,26]. The pulse fluence of 1.3 nJ cm^{-2} and corresponding peak intensity of 2.6×10^7 W m^{-2} for threshold photoemission here agrees very well with the values obtained using a femtosecond amplified laser at low repetition rates of approximately 0.7 nJ cm^{-2} and 4.6×10^7 W m^{-2} (for 1PPE) [19]. In terms of peak intensity, our results are also roughly comparable to those at synchrotron sources using picosecond X-ray pulses, where peak intensity thresholds of approximately 1.8×10^8 W m^{-2} and 4.0×10^6 W m^{-2} were determined for non- and aberration-corrected PEEM systems, respectively [24,25]. The high overall photon flux at this pulse fluence demonstrates that oscillator lasers in the 80 MHz range can achieve a reasonable balance of low electron flux (to minimize space charge) and good throughput (signal).

For the PEEM instrument used here, the electron energy in the microscope column does not change, as an in-line magnetic prism is used for energy filtering [29]. Hence, there should not be appreciable electron spatial overlap after the first crossover in the objective lens. However, we find that the pulse fluence and peak intensity for femtosecond pulses where space charge becomes significant is comparable to results from instruments with different electron-optical designs [19,24–26]. Therefore, we presume that the most significant contributions to space charge should be during the initial acceleration of the photoelectrons from the sample surface and at the first crossover at the objective lens, up to the entrance slit of the magnetic prism array.

Consequently, the useable 4ω intensity is still strongly limited by space charge at an 80 MHz laser repetition rate. However, for most PEEM experiments the practical intensity is sufficient. For example, using the 4ω at this power level (e.g. 10^{-5} W), we find that we are able to measure photoemission spectra with modest detector voltages (< 1500 V) and image acquisition times (< 5 min total) using the smallest selected area aperture (≈ 1.85 μm of sample) and narrowest energy filter (≈ 175 meV) in our PEEM system. Similarly, in imaging mode, we find that there is sufficient photoemission intensity at this limit for all but the most restrictive imaging conditions (e.g., small contrast and energy apertures). In addition, it should be possible to increase the useful photon flux in high-magnification imaging by reducing the 4ω spot size at the sample [26], which could be achieved by expanding the 4ω beam before it is focused by the lens at the PEEM window.

3.2.2. PEEM imaging and spatial resolution

After characterizing the effects of space charge using the 4ω laser, we turn now to discuss using the 4ω for real space imaging in PEEM. We first show a PEEM image of a cleaned GaN surface taken with a traditional Hg lamp in Fig. 4a. GaN is a wide-bandgap semiconductor that is becoming more prevalent in consumer electronics due to the electrification of

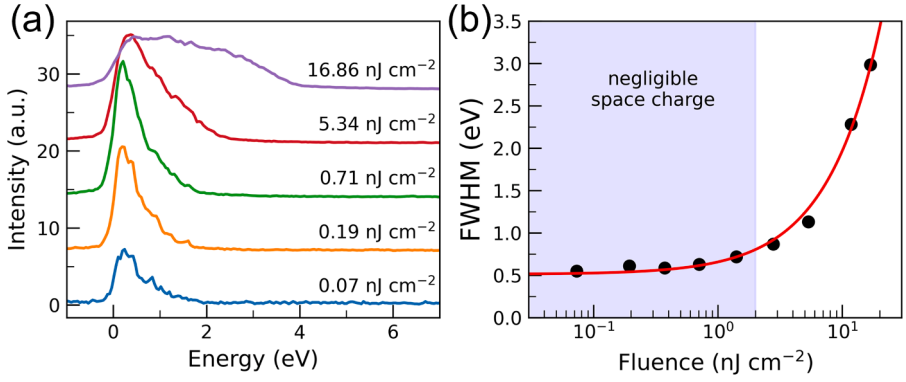

Fig. 3. Space charge effects in PEEM. a) Dispersive-mode photoemission spectra at various 200 nm (6.2 eV) 4ω fluences. The spectra were manually aligned to the low energy edge of the spectrum and are offset vertically for visibility. b) Photoemission spectra FWHM as a function of laser fluence. The red line is a linear fit to the data, as a guide to the eye.

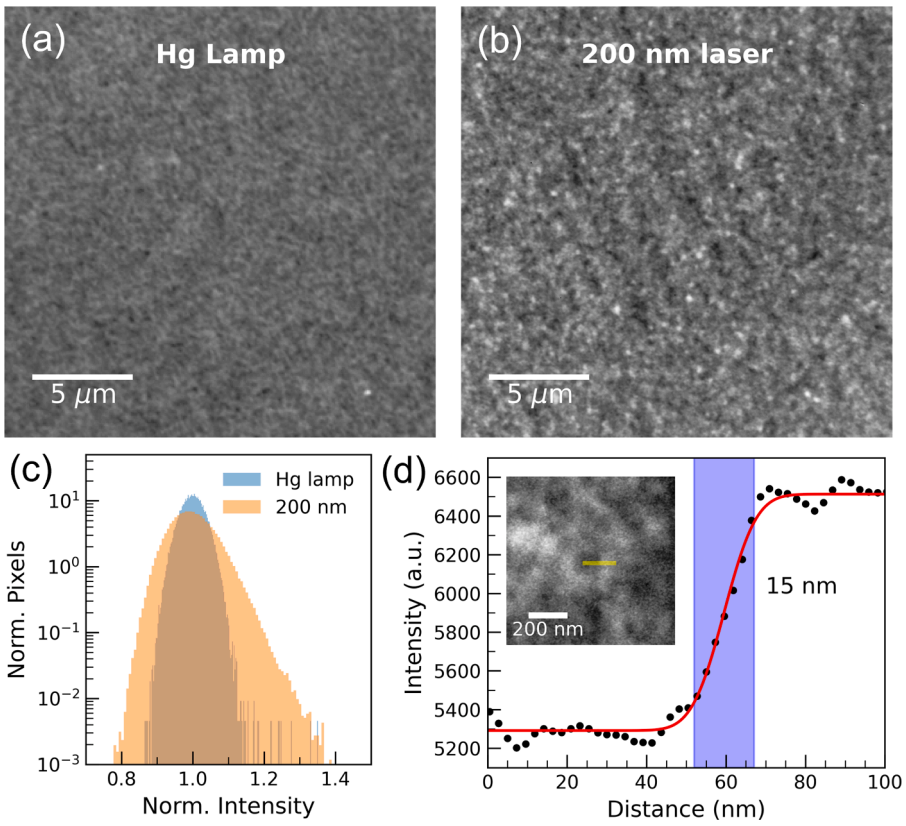

Fig. 4. PEEM imaging. Representative image of a GaN surface a) using a non-monochromatic Hg lamp and b) using the 200 nm 4ω laser-based source. The image intensity range of b) (after correction by exposure time and detector gain) is scaled to be 60 × that in a). c) Normalized intensity histograms of the images in a) and b). d) Line profile along the yellow rectangle in the high-magnification inset image. The red line is a fit to an error function, giving a width of 15 nm (shaded blue box).

energy and the increased reliance on power and high frequency devices and components [33–35]. GaN has an IP greater than 6 eV [36]; hence, the photoemission intensity using the Hg lamp is negligible and it is difficult to observe surface features. This is due to the shortest characteristic emission wavelength of the Hg lamp being approximately 255 nm (4.8 eV). Using the 4ω laser at 200 nm (6.2 eV) results in a qualitatively different PEEM image, as shown in Fig. 4b. A much more detailed topography can be observed, with many small bright and dark patches. The image contrast arises from small topographic features that cause a different photoemission yield due to the photon energy being close to the IP of GaN. The distribution of pixel intensities in the PEEM image is significantly broader using the 4ω laser at 200 nm (6.2 eV) than the Hg lamp, as shown in Fig. 4c. This is due to the larger photon energy of the 4ω laser, which can overcome the IP of GaN and emit both primary and secondary electrons. The 4ω fluence used here was 0.37 nJ cm^{-2}, below the onset of significant space charge, yet the total photoemission intensity was roughly 60 × higher than the image generated by the Hg lamp. Thus, we find that the DUV laser system allows for PEEM studies of semiconducting systems with wide and ultrawide bandgaps.

Going to higher magnification, we find that the bright and dark patches are on the order of ten to a few hundred nanometers in size, as shown in the inset of Fig. 4d. We estimate the spatial resolution of the PEEM to be 22 nm ± 5 nm from the average of three line profiles fit to an error function across different patches, one of which is shown in Fig. 4d. This spatial resolution is improved over our previous report using the Hg lamp for illumination [30]. Importantly, this shows that a higher repetition rate laser source can push the spatial resolution closer to the theoretical limit for PEEM, which was not possible for early attempts using low repetition rate lasers with high pulse energies [19,21,22]. Space charge is still expected to be one of the resolution limiting factors in PEEM [24,25], therefore the development of even higher repetition rate (or near continuous wave) DUV lasers will be required to bring the spatial resolution of PEEM towards the theoretical limit of the electron optics.

3.3. Outlook on laser-based PEEM

We have shown the initial results of coupling a pulsed femtosecond DUV laser system to a PEEM, and these results were achieved within (6) months of the laser system installation. This was largely accomplished due to the technological maturity of Ti:sapphire oscillators and to the environmental controls where the instrument is located. While we did not observe any appreciable beam drift affecting our results, the long term stability of this type of instrument would greatly benefit from automated and in-line diagnostics of the 4ω output power and spectrum to correct laser fluctuations and drift during long or low photoemission yield PEEM measurements. Overall, this successful demonstration shows the accessibility of integrating pulsed laser systems to a PEEM and allows for more advanced non-linear optical systems (e.g., high harmonic generation) to be paired to the PEEM in the future.

Looking forward, the flexibility of pulsed laser sources allows for potential expansion and modification of the optical setup to realize different PEEM measurement modalities. Changing the photon wavelength affects the emitted electron kinetic energy, which can be used to enhance PEEM imaging contrast due to the information depth, photoionization cross sections, and variations in composition and electronic structure. For example, the tuning range of the UV light could be expanded by using different harmonic generation crystals, optics, and schemes. Non-linear multi-photon photoemission measurements, where multiple identical photons are absorbed simultaneously to eject a photoelectron, have been used extensively to probe plasmonic structures [12–14,17,18] and exploit anisotropic dipole selection rules [11,15]. In our set up, this could be achieved by using intense ω, 2ω, or 3ω light, depending on the electronic structure of the system under investigation.

The pulsed nature of the laser source also allows for potential two-color time-resolved experiments with sub-picosecond time resolution for studying the relaxation or propagation of photoexcited carriers which have been widely pursued by other research groups [7,8,12–14,37–40]. For our current setup, we could conceivably use residual ω or 2ω light to pump a sample, then probe it using either 3ω or 4ω UV light, giving us the possibility to selectively excite and probe different electronic states near the Fermi level. In the near term, we are interested in applying non-linear photoemission methods to image microscopic-scale defects in semiconductors used for power electronics to disentangle topographic and electronic effects.

4. Conclusions

Here, we have shown the first results of a unique, ultrafast laser-based tunable DUV light source for PEEM applications. The high-repetition rate laser and harmonics generation module provide an intense source of UV radiation tunable between 192 nm and 210 nm (6.5 eV to 5.9 eV). The high repetition rate of the laser helps to minimize issues with space charge, such that a large photon flux (10^{13} photon s^{-1}) can be utilized for high resolution imaging and micro-spectroscopy experiments. We also show the superiority of the DUV laser source in imaging wide bandgap GaN compared to a conventional arc source, which demonstrates the extended utility of measuring and imaging electronic materials in a laboratory-based PEEM setting.

Declaration of Competing Interest

The authors declare that they have no known competing financial interests or personal relationships that could have appeared to influence the work reported in this paper.

Data availability

Data will be made available on request.

Acknowledgements

We thank Falk Niefind for discussions during the planning phase for the laser system integration.

Funding Sources

AJW was supported by the NRC Postdoctoral Associateship program. The work at NIST was supported by NIST. The work at NRL was supported by the Office of Naval Research.

References

[1] A. Locatelli, L. Aballe, T.O. Mentes, M. Kiskinova, E. Bauer, Photoemission electron microscopy with chemical sensitivity: SPELEEM methods and applications, Surf. Interface Anal. 38 (2006) 1554–1557.
[2] T.O. Menteş, G. Zamborlini, A. Sala, A. Locatelli, Cathode lens spectromicroscopy: methodology and applications, Beilstein J. Nanotechnol. 5 (2014) 1873–1886.
[3] J.J. Yeh, I. Lindau, Atomic subshell photoionization cross sections and asymmetry parameters: $1 \leqslant Z \leqslant 103$, At. Data Nucl. Data Tables 32 (1985) 1–155.
[4] X. Zhou, et al., New developments in laser-based photoemission spectroscopy and its scientific applications: a key issues review, Reports Prog. Phys. 81 (2018), 062101.
[5] J. Ringling, G. Korn, J. Squier, O. Kittelmann, F. Noack, Tunable femtosecond pulses in the near vacuum ultraviolet generated by frequency conversion of amplified Ti:sapphire laser pulses, Opt. Lett. 18 (1993) 2035.
[6] F. Rotermund, V. Petrov, Generation of the fourth harmonic of a femtosecond Ti: sapphire laser, Opt. Lett. 23 (1998) 1040.
[7] M.K.L. Man, et al., Imaging the motion of electrons across semiconductor heterojunctions, Nat. Nanotechnol. 12 (2017) 36–40.
[8] Z. Xue, et al., Photoexcited Electron Dynamics in Cd3As2 Revealed by Time- and Energy-Resolved Photoemission Electron Microscopy, J. Phys. Chem. C 126 (2022) 3134–3139.
[9] T.E. Beechem, S.W. Smith, R.G. Copeland, F. Liu, T. Ohta, Spectral and polarization based imaging in deep-ultraviolet excited photoelectron microscopy, Rev. Sci. Instrum. 93 (2022), 053701.
[10] K. Fukumoto, et al., Imaging the defect distribution in 2D hexagonal boron nitride by tracing photogenerated electron dynamics, J. Phys. D. Appl. Phys. 53 (2020).
[11] A. Neff, F. Niefind, B. Abel, S.C.B. Mannsfeld, K.R. Siefermann, Imaging nanoscale morphology of semiconducting polymer films with photoemission electron microscopy, Adv. Mater. 29 (2017), 1701012.
[12] P. Kahl, et al., Direct observation of surface plasmon polariton propagation and interference by time-resolved imaging in normal-incidence two photon photoemission microscopy, Plasmonics 13 (2018) 239–246.
[13] Q. Sun, et al., Dissecting the few-femtosecond dephasing time of dipole and quadrupole modes in gold nanoparticles using polarized photoemission electron microscopy, ACS Nano 10 (2016) 3835–3842.
[14] J.-H. Zhong, et al., Nonlinear plasmon-exciton coupling enhances sum-frequency generation from a hybrid metal/semiconductor nanostructure, Nat. Commun. 11 (2020) 1464.
[15] P.P. Joshi, R. Li, J.L. Spellberg, L. Liang, S.B. King, Nanoimaging of the edge-dependent optical polarization anisotropy of black phosphorus, Nano Lett. 22 (2022) 3180–3186.
[16] T. Taniuchi, Y. Kotani, S. Shin, Ultrahigh-spatial-resolution chemical and magnetic imaging by laser-based photoemission electron microscopy, Rev. Sci. Instrum. 86 (2015).
[17] M. Aeschlimann, et al., Spatiotemporal control of nanooptical excitations, Proc. Natl. Acad. Sci. 107 (2010) 5329–5333.
[18] M. Dąbrowski, Y. Dai, H Petek, Ultrafast microscopy: imaging light with photoelectrons on the nano-femto scale, J. Phys. Chem. Lett. 8 (2017) 4446–4455.
[19] N.M. Buckanie, et al., Space charge effects in photoemission electron microscopy using amplified femtosecond laser pulses, J. Phys. Condens. Matter 21 (2009).
[20] S. Passlack, et al., Space charge effects in photoemission with a low repetition, high intensity femtosecond laser source, J. Appl. Phys. 100 (2006), 024912.
[21] A. Mikkelsen, et al., Photoemission electron microscopy using extreme ultraviolet attosecond pulse trains, Rev. Sci. Instrum. 80 (2009).
[22] S.H. Chew, et al., Time-of-flight-photoelectron emission microscopy on plasmonic structures using attosecond extreme ultraviolet pulses, Appl. Phys. Lett. 100 (2012) 1–5.
[23] B.J. Siwick, J.R. Dwyer, R.E. Jordan, R.J.D. Miller, Ultrafast electron optics: propagation dynamics of femtosecond electron packets, J. Appl. Phys. 92 (2002) 1643–1648.
[24] A. Locatelli, T.O. Menteş, M.Á. Niño, E. Bauer, Image blur and energy broadening effects in XPEEM, Ultramicroscopy 111 (2011) 1447–1454.
[25] T. Schmidt, A. Sala, H. Marchetto, E. Umbach, H.-J. Freund, First experimental proof for aberration correction in XPEEM: resolution, transmission enhancement, and limitation by space charge effects, Ultramicroscopy 126 (2013) 23–32.
[26] D. Wilson, et al., On space charge effects in laboratory-based photoemission electron microscopy using compact gas discharge extreme ultraviolet sources, New J. Phys. 22 (2020), 103019.
[27] The identification of commercial equipment or vendor is not intended to imply recommendation or endorsement by NIST, nor is it intended to imply that the materials or equipment identified are necessarily the best available for the purpose.
[28] R.M. Tromp, M.C Reuter, Design of a new photo-emission/low-energy electron microscope for surface studies, Ultramicroscopy 36 (1991) 99–106.
[29] R.M. Tromp, et al., A simple energy filter for low energy electron microscopy/photoelectron emission microscopy instruments, J. Phys. Condens. Matter 21 (2009), 314007.
[30] F. Niefind, et al., Imaging and measuring the electronic properties of epitaxial graphene with a photoemission electron microscope, J. Appl. Phys. 131 (2022), 015303.
[31] Y. Yang, et al., Epitaxial graphene homogeneity and quantum Hall effect in millimeter-scale devices, Carbon N. Y. 115 (2017) 229–236.
[32] J.C. Gallagher, et al., Optimizing performance and yield of vertical GaN diodes using wafer scale optical techniques, Sci. Rep. 12 (2022) 658.
[33] J.Y. Tsao, E.F. Schubert, R. Fouquet, M. Lave, The electrification of energy: long-term trends and opportunities, MRS Energy Sustain. 5 (2018) 5.
[34] H. Amano, et al., The 2018 GaN power electronics roadmap, J. Phys. D. Appl. Phys. 51 (2018), 163001.
[35] J.Y. Tsao, et al., Ultrawide-bandgap semiconductors: research opportunities and challenges, Adv. Electron. Mater. 4 (2018), 1600501.
[36] V.M. Bermudez, The fundamental surface science of wurtzite gallium nitride, Surf. Sci. Rep. 72 (2017) 147–315.
[37] E.L. Wong, et al., Pulling apart photoexcited electrons by photoinducing an in-plane surface electric field, Sci. Adv. 4 (2018).
[38] T.A.S. Doherty, et al., Performance-limiting nanoscale trap clusters at grain junctions in halide perovskites, Nature 580 (2020) 360–366.
[39] S. Kosar, et al., Unraveling the varied nature and roles of defects in hybrid halide perovskites with time-resolved photoemission electron microscopy, Energy Environ. Sci. 14 (2021) 6320–6328.
[40] L. Wang, C. Xu, M.Y. Li, L.J. Li, Z.H. Loh, Unraveling spatially heterogeneous ultrafast carrier dynamics of single-layer wse2 by femtosecond time-resolved photoemission electron microscopy, Nano Lett. 18 (2018) 5172–5178.